Strong superchiral fields and an ultrasensitive chiral sensor of biomolecules based on a dielectric photonic crystal slab with air holes

Tong Wu,[*] Saisai Hou,[*] Weixuan Zhang, and Xiangdong Zhang [†]

Key Laboratory of Advanced Optoelectronic Quantum Architecture and Measurements of Ministry of Education, Beijing Key Laboratory of Nanophotonics & Ultrafine Optoelectronic Systems, School of Physics, Beijing Institute of Technology, 100081 Beijing, China

Detection and quantification of chiral enantiomers of biomolecules are of considerable importance for biomedical diagnostics and pathogen analyses. However, the chiral signals from natural molecules are typically small and weak; a long measuring time and a large amount of samples are needed to fulfill the detection limit for the present technique. How to improve the detection efficiency for realizing ultrasensitive probing of chiral molecules has become a key problem. Here we propose a scheme to perform ultrasensitive detection of chiral molecules based on degeneracy states of orthogonal polarization modes in the achiral dielectric nanostructure. The degeneracy states are realized by designing dielectric photonic crystal slabs with air holes. Based on such degeneracy states, homogeneous superchiral fields of both handedness over arbitrarily large areas can be obtained in a wide spectral range, resulting in the enhancement of the circular dichroism signal by more than three orders of magnitude, thus paving the road toward ultrasensitive characterization and quantification of molecular chirality.

I. INTRODUCTION

Chiral molecules are pervasive in daily life: from sugars, to naturally occurring amino acids, to proteins. As with hands, chiral molecules can occur in two different forms, called enantiomers, which are mirror images of one another. The enantiomeric molecules often share the same physical and chemical properties but exhibit different behaviors in chiral environments. Thus, the detection and characterization of their different enantiomers are of considerable importance for the modern biochemical and pharmaceutical industries [1,2]. To determine the chirality of molecules, one often resorts to circular dichroism (CD) spectroscopy, which detects the absorption of light by molecules incident by left- (LCP) and right-circular polarized (RCP) lights [3–5]. For most natural chiral molecules, the chiral optical response is typically small and weak, which is usually three orders of magnitude smaller than its parent absorption intensities. Usually, a long measuring time (around 30 min) and high analyte concentrations are required to guarantee the accuracy and stability of the measurement. In this context, how to improve the detection efficiency for realizing ultrasensitive probing of chiral molecules has become a problem of intense interest in recent years.

Previous investigations have focused on enhancing the CD signal with chemical synthesized simple colloidal plasmonic particles, such as nanorods, gold nanosphere clusters, or silver nanocubes [6–29]. However, for these structures, the pure handedness of the LCP and RCP waves are not preserved, leading to regions of different helicities existing in the near fields. This also results in lower overall optical chirality $C = -\frac{\varepsilon_0 \omega}{2} \mathrm{Im}(\mathbf{E}^* \cdot \mathbf{H})$ [30–35]. Here, $\mathbf{E}$ and $\mathbf{H}$ represent the complex electric and magnetic fields, and ω is the angular frequency of the light. Consequently, the molecular induced CD, proportional to C, is only weakly enhanced by the plasmonic nanoparticles. Notably, a recent work has shown that a single-handed optical chirality near field can be generated on an achiral cavity-coupled plasmonic system by designing the structure carefully in order to overlap "magnetic"- and "electric"-like modes [36]. In addition, some specifically designed structures such as double split ring resonators or nanostructures consisting of multiple helices may provide an overall enhancement of the optical chirality field [25,37–40]. However, most of these designs mainly operate in the infrared or midinfrared region, which greatly limits their use in CD. Furthermore, CD enhanced by plasmonic structure suffers from high optical losses in metallic elements. The optical losses induce a giant photothermal effect, which leads to denaturation of the analytes and affects the quality and reliability of the CD spectrum [28,29].

On the other hand, the dielectric structures have been extensively studied for the purpose of enhancing the optical chirality field [41–49]. In contrast to most plasmonic structures which always destroy the polarization of the incident wave, dielectric structures such as nanospheres, nanorods, dielectric metasurface, and specifically designed one-dimensional photonic crystal have the capability for preserving the chirality of the incident light [26,50–52]. The physics behind the phenomenon is that these dielectric structures respond equally to the TE and the TM polarized incident waves, making them become helicity preserving structures [51,52]. However, for most dielectric structures

---

[*]These authors contributed equally to this work.

[†]zhangxd@bit.edu.cn

such as nanospheres, the enhancement of C remains relatively low [26,50], especially the spatial averaging enhancement, which is several to dozens of times compared with circular polarized light (CPL). Although the local and the average optical chirality field enhancements of the dielectric disk metasurfaces can exceed 1000-fold and 400-fold, respectively [49], a large portion of electromagnetic (EM) energy is concentrated in the dielectric regions rather than the surfaces of the structures (where the analytes are adsorbed). How to make full use of this part of the energy is still a challenge.

Recently, we designed a photonic crystal (PhC) slab supporting helicity preserving exceptional points (EP) [53–55]. A large portion of EM energy concentrated in the cylindrical holes can be used to perform surface enhanced fluorescence CD and Raman optical activity of chiral molecules. But it is not a simple task to effectively excite the eigenstate of the vector EP. Although a new excited method using two beams of CPL to excite the system from opposite directions has been proposed, it is not easy to operate in practical applications.

In this work, we propose to use the dielectric PhC slab with air holes for enhancing the optical chirality field by engineering the structure to guarantee that the TE- and TM-like modes can be simultaneously excited by CPL incident in a single direction. A PhC slab supports in-plane guided modes which give rise to strong field enhancement [56]. The guided modes have a large portion of their mode volumes extending outside their dielectric region, i.e., the hole regions and the surface of the slab. The nondielectric region with a large optical chirality field can be well filled by chiral molecules [57], which greatly enhances the interaction between light and chiral molecules. By fine-tuning structural parameters of the PhC slab, such as the thickness, and the radius of the nanoholes, a quasifourfold degenerate mode can be found at the Brillouin zone center. When the mode is excited by the CPL, a giant optical chirality field can be generated. Depending on the size of the nanoholes, the spatial averaging chirality field inside the hole regions can be three orders of magnitude larger than that of the CPL. The physical origins for these phenomena have been discussed.

II. SYSTEMS AND DEGENERACY STATES OF ORTHOGONAL POLARIZATION MODES

We consider a dielectric PhC slab, consisting of a square lattice of holes embedded in air [Fig. 1(a)]. Figure 1(b) shows a unit cell of the PhC slab. The lattice constant is set as a, the thickness of the slab is taken as t, and the radius of the air holes is marked as r. The PhC slab has a refraction index $n = 2.02$ (Si_3N_4) and is immersed in a medium with refraction index $n = 1.46$. Such a structure can be fabricated using interference lithography [58]. Due to the periodicity within the XY plane, the resonance properties of the slab can be described by a photonic band structure [Fig. 1(c)]. Here, the geometric parameters of the structure are taken as $t = 200$ nm, $r = 80$ nm, and $a = 336$ nm. Considering that the PhC slab is symmetric with respect to the $z = 0$ plane, the resonance modes can be classified as TE-like (even) and TM-like (odd), which are plotted in Fig. 1(c) with blue squares and orange triangles, respectively. At the Brillouin zone center (Γ), the

structure supports both double-degenerate states and nondegenerate states. We have enlarged the plot near the Γ point in the illustration of Fig. 1(c). According to group theory, the nondegenerate modes are not coupled to radiation modes in free space [58–60]. On the other hand, the degenerate modes are a pair of eigenfunctions of the two-dimensional irreducible representation of the point group of the PhC slab ($C4v$), and can couple to the external incident optical beams. In the following, we only focus on these double-degenerate modes, because they are the only modes which can be excited by an external circular polarized plane wave used for chiral molecule detection.

Figure 1(d) shows the evolution of the double-degenerate TE-like and TM-like modes at Γ point as a function of thickness for PhC slabs with different radii of nanoholes. The double-degenerate TE-like modes are indicated by solid squares, while the double-degenerate TM-like modes are denoted by hollow squares. Other parameters of the system are set to be identical with those in Fig. 1(c). For all the cases, the eigenfrequency decreases with the increase of the thickness of the slab. If the slab is thin, then TM-like modes (hollow squares) have higher frequency. However, the eigenfrequency for the TM-like mode decreases much faster than that of the TE-like mode, and, at a certain point, the two different kinds of modes become coincident, giving rise to a quasifourfold degenerate point. By varying the thickness of the PhC slab, we can find the quasifourfold point for structures with different radii of holes. In Fig. 1(d), we connect the quasifourfold degenerate points (black solid line), and find that they form a parabolic line in the parameter space of frequency and thickness. This phenomenon arises from the competition between influences on frequency shift due to thickness and radius changes, and can be understood from a modal perturbation theory [61] (see Sec. S1 in the Supplemental Material [62] for a detailed discussion). As we will show below, the quasifourfold degenerate point promises not only an ultrastrong light confinement but also a large optical chirality inside the hole regions.

To reveal why the quasifourfold degenerate states may favor a large optical chirality, in Figs. 2(a) and 2(b) we plot the distributions of electric and magnetic fields for the double-degenerate TM- and TE-like modes in a unit cell, respectively. For the double-degenerate eigenmodes, the field distribution of one mode can be obtained from the other through a $\pi/2$ rotation. For example, the $|\tilde{\mathbf{E}}|$ or $|\tilde{\mathbf{H}}|$ distribution of one mode on the XZ plane is the same as that of the other mode on the YZ plane. Thus, both of the two double-degenerate eigenmodes have the distribution of electric and magnetic fields shown in Fig. 2, which are manifested in different planes. For concision, we only show the eigenfields of one mode in the text. Furthermore, we present the top view of maps for the electric and magnetic fields in Sec. S2 of the Supplemental Material [62]. The red (blue) arrows in Fig. 2 denote the real part of the electric (magnetic) fields in space. Though sharing the same symmetry in the XY plane, the electric and magnetic profiles of the degenerate modes of TE-like and TM-like solutions are in sharp contrast with each other. Specifically, the electric fields for the TE-like mode are most intense at the center region of the nanohole while the electric fields for the TM-like mode are circulating in the dielectric region. Because
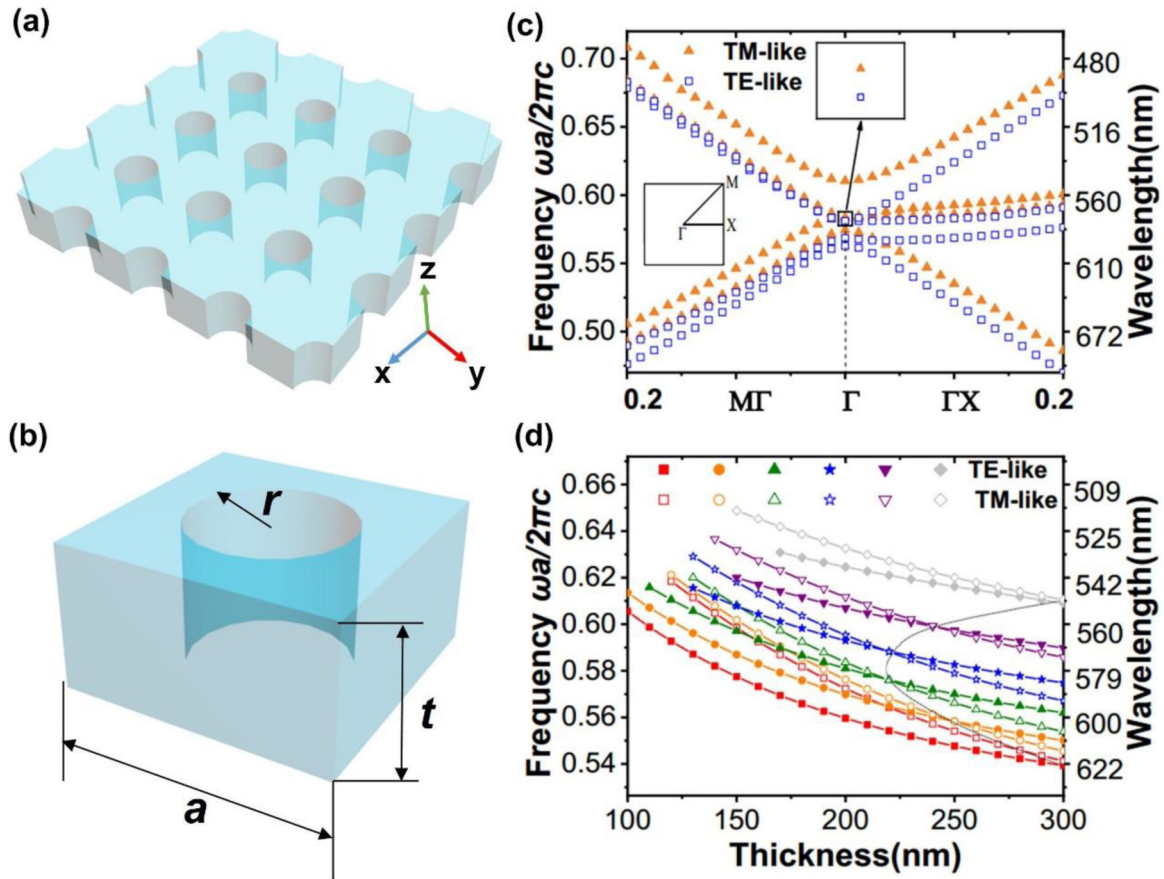
FIG. 1. (a) Schematic plot of the PhC slab. (b) A unit cell for the PhC slab. The lattice constant is set as a, the thickness is taken as t, and the radius of the nanohole is equal to r. (c) Dispersion relation around the frequency $f = 0.6c/a$ in the ΓX and ΓM directions as a function of Bloch wave vector (in unit of π/a), where c is the vacuum speed of light. TM-like and TE-like modes are denoted by orange triangles and blue squares, respectively. (d) Evolution of the double-degenerate TE-like and TM-like modes at the Γ point as a function of thickness. The red (square), orange (circle), green (triangle), blue (star), purple (inverted triangle), and gray (rhombus) lines correspond to the cases of $r = 40$, 60, 80, 100, 120, and 140 nm, respectively.

magnetic field is a pseudovector, its symmetry with respect to the $z = 0$ nm plane is opposite to that of electric field, as can be seen by comparing the directions of $\tilde{\mathbf{E}}$ with those of $\tilde{\mathbf{H}}$ in Figs. 2(a) and 2(b). According to the definition of the optical chirality, $C = -\frac{\varepsilon_0 \omega}{2} \text{Im}(\mathbf{E}^* \cdot \mathbf{H})$, interaction between light and chiral molecules should reach maximum when electric field and magnetic field are both significantly enhanced at the same position and have a parallel component with the difference phase of $\pi/2$. From the distributions of $\tilde{\mathbf{E}}$ and $\tilde{\mathbf{H}}$ fields in Figs. 2(a) and 2(b), we can expect that the PhC slab would not give rise to extremely large superchiral fields if only a single pair of TM-like or TE-like modes is excited. This is because, firstly, the region where the electric fields have large values does not overlap with that of the magnetic fields, and, more importantly, the electric fields are nearly perpendicular with the magnetic fields. These issues can be solved with the quasifourfold degenerate state where TM-like and TE-like modes spectrally coincide and can be simultaneously excited.

Besides depicting the vector diagrams for the electric and magnetic fields of eigenmodes, the emergence of a large optical chirality field can also be understood by computing the helicity field when the structure is excited by a CPL.

For complex EM fields, the eigenstates of the helicity are given by $\mathbf{G}_\pm = 1/\sqrt{2}(\mathbf{E} \pm iZ\mathbf{H})$, with Z being the impedance and $\pm$ denoting the eigenvalues $+1$ and -1. According to Ref. [63], the optical chirality is proportional to the difference between the intensities of these two helicity eigenvectors; i.e., $C \propto |\mathbf{G}_+|^2 - |\mathbf{G}_-|^2$. Figures 3(a), 3(c), and 3(e) show the distributions of $|\mathbf{E} + iZ\mathbf{H}|^2$ with various slab thicknesses, which have the helicity eigenvalue $+1$ equaling that of the incident CPL. The corresponding results for $|\mathbf{E} - iZ\mathbf{H}|^2$ with the opposite helicity are given in Figs. 3(b), 3(d), and 3(f). Here the thicknesses of the PhC slabs in Figs. 3(a) and 3(b), 3(c) and 3(d), and 3(e) and 3(f) are taken as $t = 160$, 218.6, and 280 nm, respectively. The lattice constant of the slab is set as 336 nm, and the radius of the nanoholes is 80 nm. The slabs are illuminated with the CPL at the wavelengths of 557.2 nm [Figs. 3(a) and 3(b)], 582.5 nm [3(c) and 3(d)], and 594.4 nm [3(e) and 3(f)], which correspond to the engenfrequencies of TM-like degenerate modes, quasifourfold degenerate mode, and TE-like degenerate modes.

As shown in Figs. 3(a) [3(b)] and 3(e) [3(f)], only a single pair of TM-like or TE-like modes can be excited. Consequently, the difference between $|\mathbf{G}_+|^2$ and $|\mathbf{G}_-|^2$ is small, which gives rise to weak optical chirality intensity. On
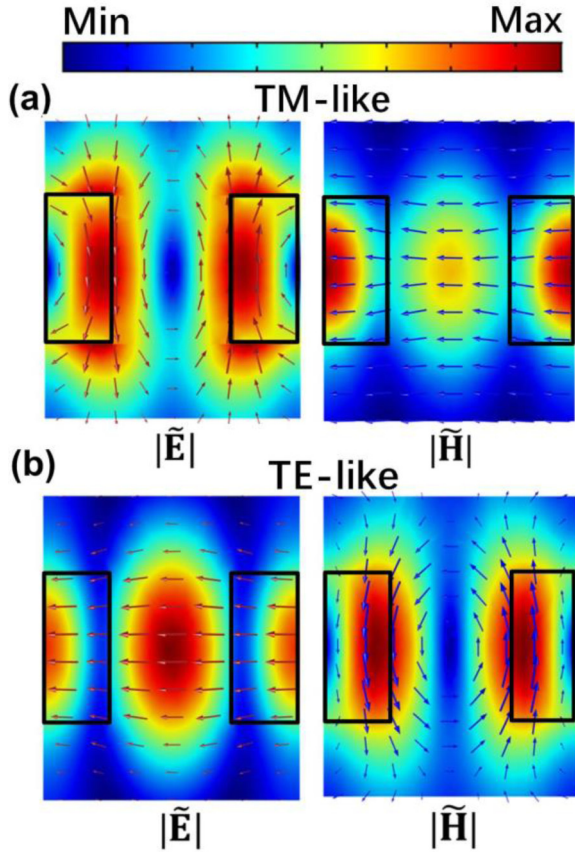
FIG. 2. (a) The distributions of electric and magnetic fields for the double-degenerate TM-like mode at the frequency of $0.584c/a$ in a unit cell. (b) The distributions of electric and magnetic fields for the double-degenerate TE-like mode at the frequency of $0.581c/a$ in a unit cell. The red (blue) arrows denote the real part of the electric (magnetic) fields in space. The Si_3N_4 of the unit cell is framed by the black solid line. The parameters of the PhC slab in this figure are the same as in Fig. 1(c).
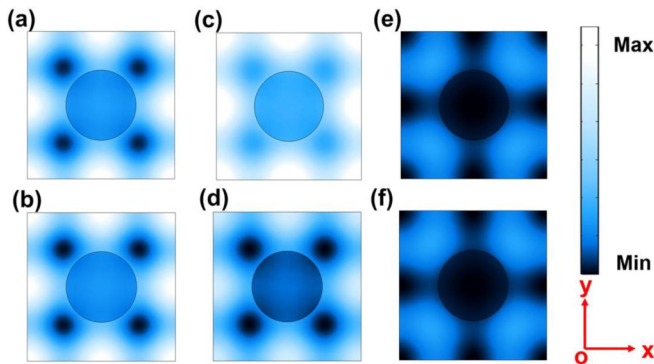

FIG. 3. The intensities of two helicity components for PhC slabs with different thicknesses. Panels (a), (b), (c), (d), and (e), (f) correspond to the cases where $t = 160$ nm, $t = 218.6$ nm, and $t = 280$ nm, respectively. (a), (c), (e) correspond to the distribution of $|G_+|^2$, which has helicity eigenvalue $+1$ equal to that of the incident plane wave; (b), (d), (f) are for the $|G_-|^2$, which has helicity eigenvalue -1 equal to that of the incident plane wave. The wavelengths of the incident light are set to be (a), (b) 557.2 nm, (c), (d) 582.5 nm, and (e), (f) 594.4 nm. The radius of the nanoholes is $r = 80$ nm, and the lattice constant is set as $a = 336$ nm.

the other hand, for a slab with TM-like modes and TE-like modes crossing at the same frequency (the case in Fig. 3(c) [3(d)]), the difference between $|G_+|^2$ and $|G_-|^2$ is large, and consequently, a giant optical chirality field is generated. In the following, we will see when such a quasifourfold degenerate state is excited by the CPL, optical chirality is improved dramatically. Here, it is worth stressing that, because the PhC slab is achiral, it is not difficult to imagine if we reverse the helicity of the incident wave, i.e., change the handedness of its polarization, the value of $|G_+|^2$ and $|G_-|^2$ will be reversed, leading to an opposite chirality field. Since the dominant component of the eigenvectors is always the same as that of the incident light, this means that our designed PhC slab has the function of preserving helicity.

III. STRONG SUPERCHIRAL FIELDS AND ULTRASENSITIVE CHIRAL SENSOR OF BIOMOLECULES

In order to verify the theory above and evaluate the potential of the resonance modes in enhancing the interaction between light and chiral molecules, we calculate the averaged enhancements of electric field intensity ($\int_V |\mathbf{E}|^2/|\mathbf{E}_0|^2 dV$), magnetic field intensity ($\int_V |\mathbf{H}|^2/|\mathbf{H}_0|^2 dV$), and optical chirality ($\int_V C/C_0 dV$) for the PhC slabs in the case of CPL incidence. Here, V denotes the volume of the nanoholes of the PhC slab, which can be occupied by chiral molecules in the real experiment. $\mathbf{E}_0$, $\mathbf{H}_0$, and C_0 represent the electric field, magnetic field, and optical chirality of the incident CPL, respectively. Figures 4(a)–4(c) show the spatially averaged electric ($|\mathbf{E}|^2/|\mathbf{E}_0|^2$), magnetic ($|\mathbf{H}|^2/|\mathbf{H}_0|^2$), and optical chirality (C/C_0) enhancement factors for PhC slabs with various thicknesses at $r = 80$ nm. Here we show the results for cases with $t = 160$, 190, 250, 280, and 218.6 nm. The lattice constant of the PhC slab is set as $a = 336$ nm. Except for the case where $t = 218.6$ nm, one can observe two peaks in Fig. 4(a). The emulation of the broader peak (e.g., at $\lambda = 567$ nm when $t = 160$ nm) in Fig. 4(a) is attributed to the excitation of the TE-like mode, while the narrower peak (e.g., at $\lambda = 558$ nm when $t = 160$ nm) is caused by the excitation of the TM-like mode. Because the TM-like mode has a longer resonance lifetime and higher Q value, its enhancement of the electric field is always larger than that of the TE-like mode, especially when the slab is thin. With the thickness increase of the PhC slab, the electric field enhancement factors for the two modes approach each other and finally both reach a value of 350-fold at $t = 280$ nm. In contrast to the electric field enhancement, from Fig. 4(b), the magnetic field intensity for the TM-like mode is overwhelmingly enhanced. For example, as indicated by the red line in Fig. 4(b), the averaged magnetic field for excitation of the TM-like mode is around 16 times larger than that at TE-like resonance frequency. Such a large magnetic field enhancement is caused by the circulating displacement current inside the dielectric region of the slab when it is at the TM-like resonance frequency.

Since the optical chirality depends on the intensity of both electric field and magnetic field, the optical chirality is not likely to be significantly enhanced at the TE-like mode resonance frequency. Indeed, from Fig. 4(c), the optical chirality is only slightly enhanced when $t = 250$ nm (at $\lambda = 589$ nm) and $t = 280$ nm (at $\lambda = 593$ nm). For slabs with thinner thickness,
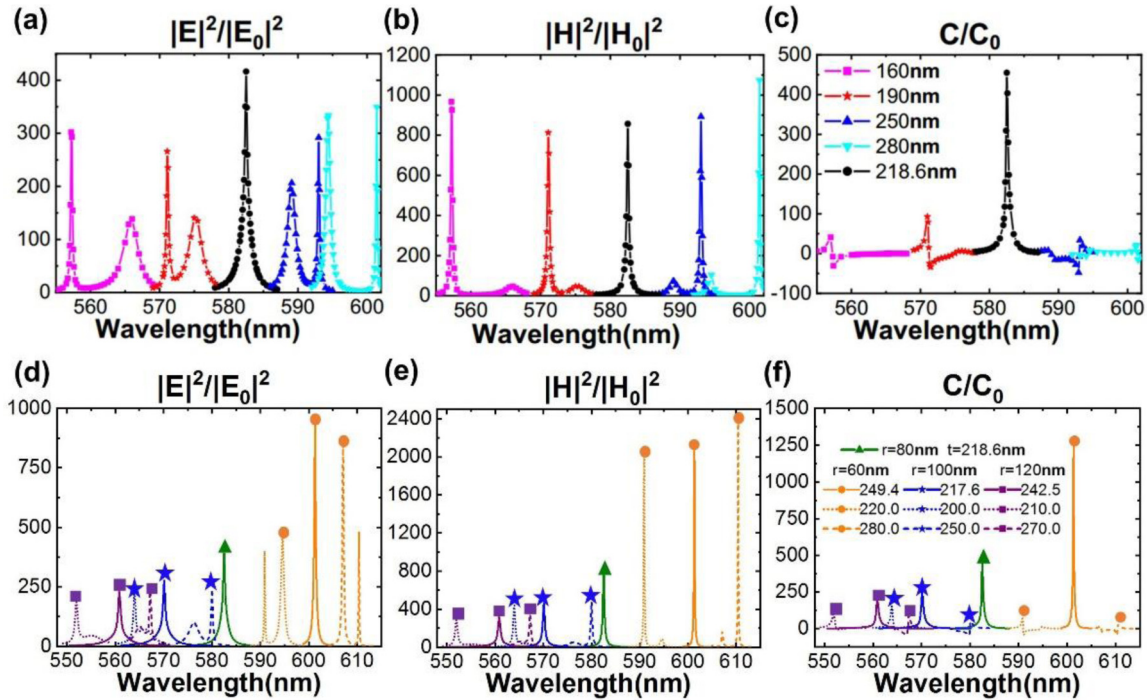
FIG. 4. (a)–(c) Spatially averaged electric, magnetic, and optical chirality enhancement factors of the PhC slabs with different thicknesses. The lattice constant of the PhC slabs is set as $a = 336$ nm, while the radius of the nanoholes is taken as $r = 80$ nm. (d)–(f) Spatially averaged electric field, magnetic field, and optical chirality enhancement factors of the PhC slabs with different thicknesses and radii. The lattice constant of the PhC slab is set as $a = 336$ nm.

such as $t = 190$ nm, one cannot observe any peak related to the TE-like resonance. In contrast, Fano resonances near the TM-like mode frequency can be found for all the slabs discussed above. The maximum enhancement factor reaches 100 at $t = 190$ nm. However, comparing Fig. 4(c) with Fig. 4(a) or 4(b), it is obvious that the enhancement factor for optical chirality is much smaller than that of the electric or magnetic field. For example, when $t = 160$ nm, the enhancement factors for the electric and magnetic fields are 300-fold and 1000-fold, respectively, while the optical chirality only reaches a value of 50. As mentioned above, this is because the electric and magnetic fields are nearly perpendicular with each other.

This issue can be elegantly solved by fine-tuning the thickness of the PhC slab, and constructing a quasifourfold degenerate state discussed above. The black circles in Figs. 4(a)–4(c) show the enhancement factors of electric field, magnetic field, and optical chirality field of the PhC slab ($t = 218.6$ nm) with the above quasifourfold degenerate state. Because the modes are degenerated, only one peak can be observed in all of these figures. From Figs. 4(a) and 4(b), the enhancement factors for the electric and magnetic fields are close to those of the other slabs. However, according to Fig. 4(c), we find the averaged optical chirality for this slab is much larger. Specifically, the peak at $\lambda = 582.5$ nm reaches a value near 500, which is 5–10 times greater than those slabs with other thicknesses. In the experiment, the nondielectric region (nanoholes region, upper and lower surfaces of PhC slab) with a large optical chirality field of the PhC slab can be well filled by chiral molecules, which greatly enhances the interaction between light and chiral molecules.

The results in Figs. 4(a)–4(c) are only for the case with $r = 80$ nm. In fact, the enhancement of optical chirality strongly depends on the radii of nanoholes in the PhC slab. Figures 4(d)–4(f) show the averaged electric field, magnetic field, and optical chirality field for PhC slabs with different thicknesses and radii. The solid purple, blue, green, and orange lines in these figures describe the enhancements of field for slabs with overlapping TM-like and TE-like resonance modes (i.e., quasifourfold degenerate), while the dashed and dotted lines correspond to the results for slabs with separated TM- and TE-like modes. By comparing the dotted and dashed lines with the corresponding solid line (with the same color), one can find [from Fig. 4(f)] that, when the radius of nanoholes is fixed, the largest optical chirality is always generated in those slabs with degenerated TE-like and TM-like modes, despite the enhancement factors for electric and magnetic fields being close [see Figs. 4(d) and 4(e)].

From Figs. 4(d) and 4(e), it is seen clearly that the maximum enhancements of electric and magnetic fields increase rapidly with the decrease of the nanohole radius. For example, when $r = 60$ nm (orange circles), it is seen clearly that the enhancements of electric and magnetic fields reach values of 1000 and 2400, respectively, which are more than 4 times larger than those for slabs with $r = 120$ nm (purple line). Because of the coexistence of a giant electric field and magnetic field inside the nanohole, the optical chirality field is significantly improved. As can be seen from Fig. 4(f), the peak of C/C_0 reaches a value of 1250 when $r = 60$ nm. By adjusting the parameters of the PhC slab more finely, the chiral field can be improved even more. However, here it is worth to stress that such a large optical chirality is generated only because
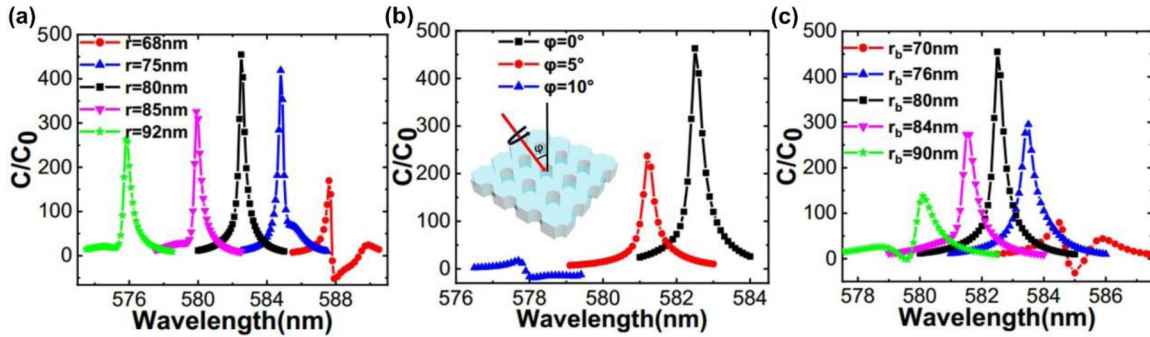
FIG. 5. (a) Optical chirality enhancement factors of the PhC slabs with different radii r. (b) Optical chirality enhancement factors of the PhC slabs with different incident angles φ. (c) Optical chirality enhancement factors of the PhC slabs with different bottom radii r_b. The top radius is fixed at 80 nm. The lattice constant a and the thickness t of the PhC slabs are set as 218.6 and 336 nm, respectively.

the PhC slab with a smaller radius of nanoholes has a larger quality factor. Consequently, the linewidth of the resonance peak for such a slab is small, making the enhancement factor of the chirality field extremely sensitive to the variation of wavelength. In contrast, for slabs with a larger hole radius, the line shape of C/C_0 is much broader.

In the real experiment, due to the imperfection of the PhC slab, the TM- and TE-like modes are not exactly overlapped. When the distance between frequencies of these two modes is larger than the linewidth of the TE-like mode (which is much broader than TM-like mode), the maximum enhancement factor for optical chirality decreases dramatically. For instance, as can be seen from Figs. 4(d) and 4(e), the slab with $r = 100$ nm and $t = 250$ nm (the blue dashed line marked with a star) has two spectrally well distinguished peaks, which correspond to the two different kinds of modes. Since the two different modes are frequently well separated, simultaneous excitation of these two modes is impossible. Only weakly enhanced optical chirality can be observed, which is clearly depicted in Fig. 4(f). On the other hand, for a slab with a large hole radius, because the TE-like mode is broader, there is a big chance for its TM-like mode to spectrally overlap with the TE-like mode, as long as the PhC slab is not too thick or thin. For such PhC slab, a large chirality field can still be generated even when TM-like and TE-like modes are not exactly degenerated. For example, the peak value of C/C_0 for a slab with $r = 120$ nm, $t = 270$ nm reaches 100, which is about half of that for a slab with $r = 120$ nm, $t = 242.5$ nm (with TM- and TE- like modes in the exact same frequency). Therefore, a slab with a larger nanohole radius has a smaller quality factor and generates a smaller optical chirality field, but it processes much broader linewidths of the modes, which makes its maximum optical chirality enhancement factor less likely influenced by the imperfection of fabrication.

To further study the variation of the optical chirality field with the breaking of the degeneracy, we consider three cases in Fig. 5. The different curves in Fig. 5(a) display optical chirality for PhC slabs with a fixed thickness but different radii. The enhancement factors decrease gradually with the radius moving away from $r = 80$ nm where the quasifourfold degenerate mode exists. Figure 5(b) studies the influence of incident angle on the optical chirality. By adjusting the an-

gles φ between the incident CPL and z axis as shown in Fig. 5(b), the optical chirality enhancement factors decrease with the increase of φ. The optical chirality only reaches a value of 17 when the angle equals $10°$. The PhC slabs in Figs. 5(a) and 5(b) both have mirror symmetry with respect to the $z = 0$ nm plane. In Fig. 5(c), the mirror symmetry is broken by changing the bottom radius r_b of the nanoholes (making the holes bear a truncated cone shape). The different lines display optical chirality enhancement factors for the PhC slabs with $r_b = 70$, 76, 80, 84, and 90 nm. Here, the top radius is fixed at 80 nm. We can find that the optical chirality enhancement factors also decrease gradually with the increase of mirror symmetry breaking. All three cases indicate that the PhC slabs with the quasifourfold degenerate mode can tolerate some perturbations, which means its optical chirality enhancement factor can always maintain a high value under some tiny disturbances.

For the above discussions, we assume that the PhC slabs are surrounded by a medium with refraction index $n = 1.46$ (the sample is immersed in oil). In molecular detection experiments, molecules are usually immersed in an aqueous solution ($n = 1.33$). In Fig. 6(a), we plot the evolution of eigenmodes as a function of thickness for the Si_3N_4 PhC slab immersed in water. The lattice constant of the PhC slab is set as $a = 336$ nm, and the radius of the nanoholes is taken as $r = 50.7$ nm. Here, the hollow red and solid blue squares correspond to the results for double-degenerated TE-like and TM-like modes, respectively. The quasidegenerate point of the TE-like and TM-like modes appears around $f = 0.555 c/a$ and $t = 280$ nm. Figure 6(b) shows the enhancement factors of the optical chirality field as a function of wavelength for the corresponding PhC slab with $t = 280$ nm. It is seen clearly that the large optical chirality field (~ 1750) is generated at the resonance frequency ($0.555 c/a$) corresponding to the quasifourfold degenerate modes as described in Fig. 6(a).

In addition, in most experimental studies the PhC slab should always be fabricated on a dielectric substrate of which the refraction index is different from that of the ambient medium. In the presence of the substrate, mirror symmetry with respect to the $z = 0$ nm plane of the structure is broken. Thus, the double-degenerate modes can no longer be assigned as TE-like and TM-like modes. However, if the
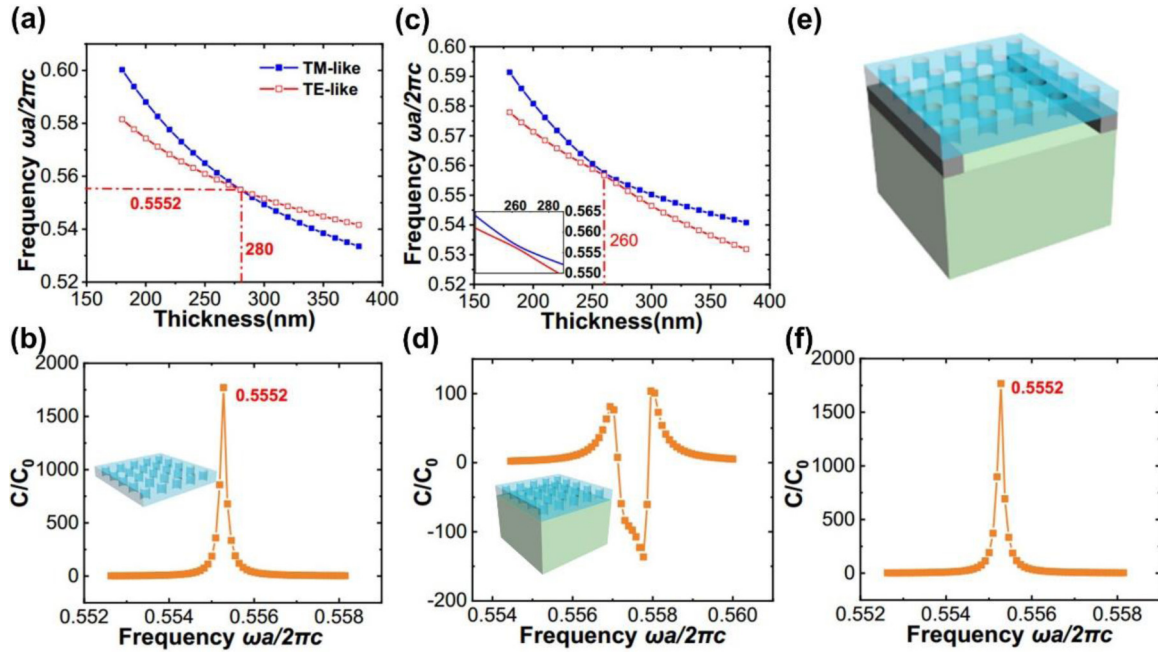
FIG. 6. (a) Evolution of eigenmodes as a function of thickness for a PhC slab immersed in water ($n = 1.33$). (b) Optical chirality enhancement factor for PhC slab with the thickness of 280 nm immersed in water. (c) Evolution of eigenmodes as a function of thickness for a PhC slab fabricated on a SiO_2 substrate ($n = 1.46$) and immersed in water. (d) The enhancement of the optical chirality field for a PhC slab with thickness 260 nm immersed in water. (e) There is a 270 nm space between the PhC slab and the substrate. (f) The evolution of optical chirality field enhancement factor as a function of wavelength for the PhC slab shown in (e). The thickness of the PhC slab is $t = 280$ nm. The lattice constant of the PhC slab is set as $a = 336$ nm, and the radius of the nanoholes is taken as $r = 50.7$ nm.

refraction index of the dielectric substrate is close to that of water, one can still find two pairs of degenerate modes the field profiles of which resemble those of TE-like and TM-like modes in symmetric structure. In analogy to Fig. 6(a), Fig. 6(c) shows the evolution of eigenmodes for the asymmetric structure where the PhC slab is fabricated on a SiO_2 substrate. We can identify the modes (marked by blue and red lines) which correspond closely to those in Fig. 6(a). Here, we name these modes as quasi-TE- and TM-like modes. From Fig. 6(c), one can find that, in contrast to the real TE- and TM-like modes, these modes only approach each other but never cross in the dispersion plane. The distance between these modes reaches its minimum at $t = 260$ nm. The curve in Fig. 6(d) corresponds to the optical chirality enhancement factor (~ 150) for such a case with a thickness $t = 260$ nm. In contrast, the optical chirality enhancement factor of a PhC slab with broken mirror symmetry is not prominent. To solve this problem, we design the structure shown in Fig. 6(e). There is a 230–410 nm spacing between the PhC slab and the substrate, which reduces the influence of the substrate effectively. Figure 6(f) shows the evolution of the optical chirality field enhancement factor with a gap of 270 nm between the PhC slab and the substrate. Here, the thickness of the PhC slab is consistent with that in Fig. 6(b). Comparing Fig. 6(f) with Fig. 6(b), it is obvious that the enhancement factor for optical chirality [Fig. 6(f)] is the same as that without the substrate [Fig. 6(b)].

IV. CONCLUSION

In conclusion, we have shown how the finely adjusted PhC slab can enhance the optical chirality field and thus the interaction between chiral molecules and light is enhanced. The double-degenerate TE-like and TM-like modes of PhC can coincide by tuning the thickness of the slab and the radius of the nanohole finely. When the mode is excited by the CPL, the optical chirality field can be improved by more than three orders of magnitude. This phenomenon can be explained by the fact that the electric field (magnetic field) of the TE-like mode has a large component parallel with the magnetic field (electric field) of the TM-like mode. This can also be attributed to the fact that the PhC slab has the property of maintaining optical helicity. Furthermore, such a phenomenon has a strong tolerance of structural parameters, which is easy to realize in the experiment by fabricating the PhC sample. Thus, our study may provide a strategy for ultrasensitive detection and quantification of molecular chirality.

[1] M. Quack, How important is parity violation for molecular and biomolecular chirality? Angew. Chem., Int. Ed. **41**, 4618 (2002).

[2] L. A. Nguyen, H. Hua, and P.-H. Chuong, Chiral drugs: An overview, Int. J. Biomed. Sci. **2**, 85 (2006).

[3] G. H. Wagnière, *On Chirality and the Universal Asymmetry: Reflections on Image and Mirror Image* (Wiley-VCH, Berlin, 2007).

[4] N. Berova, P. L. Polavarapu, K. Nakanishi, and R. W. Woody, *Comprehensive Chiroptical Spectroscopy* (John Wiley and Sons Inc, New York, 2012).

[5] D. Patterson, M. Schnell, and J. M. Doyle, Enantiomer-specific detection of chiral molecules via microwave spectroscopy, Nature **497**, 475 (2013).

[6] A. O. Govorov, Z. Fan, P. Hernandez, J. M. Slocik, and R. R. Naik, Theory of circular dichroism of nanomaterials comprising chiral molecules and nanocrystals: Plasmon enhancement, dipole interactions, and dielectric effects, Nano Lett. **10**, 1374 (2010).

[7] T. Wu, J. Ren, R. Wang, and X. Zhang, Competition of chiroptical effect caused by nanostructure and chiral molecules, J. Phys. Chem. C **118**, 20529 (2014).

[8] H. Zhang and A. O. Govorov, Giant circular dichroism of a molecule in a region of strong plasmon resonances between two neighboring gold nanocrystals, Phys. Rev. B **87**, 075410 (2013).

[9] A. O. Govorov, Plasmon-induced circular dichroism of a chiral molecule in the vicinity of metal nanocrystals. Application to various geometries, J. Phys. Chem. C **115**, 7914 (2011).

[10] A. O. Govorov and Z. Fan, Theory of chiral plasmonic nanostructures comprising metal nanocrystals and chiral molecular media, Chem. Phys. Chem. **13**, 2551 (2012).

[11] N. A. Abdulrahman, Z. Fan, T. Tonooka, S. M. Kelly, N.Gadegaard, E. Hendry, A. O. Govorov, and M. Kadodwala, Induced chirality through electromagnetic coupling between chiral molecular layers and plasmonic nanostructures, Nano Lett. **12**, 977 (2012).

[12] M. L. Nesterov, X. Yin, M. Schäferling, H. Giessen, and T. Weiss, The role of plasmon-generated near fields for enhanced circular dichroism spectroscopy, ACS Photonics **3**, 578 (2016).

[13] T. J. Davis and D. E. Gomez, Interaction of localized surface plasmons with chiral molecules, Phys. Rev. B **90**, 235424 (2014).

[14] E. Hendry, T. Carpy, J. Johnston, M. Popland, R. V. Mikhaylovskiy, A. J. Lapthorn, S. M. Kelly, L. D. Barron, N. Gadegaard, and M. Kadodwala, Ultrasensitive detection and characterization of biomolecules using superchiral fields, Nat. Nanotechnol. **5**, 783 (2010).

[15] R. Tullius, A. S. Karimullah, M. Rodier, B. Fitzpatrick, N. Gadegaard, L. D. Barron, V. M. Rotello, G. Cooke, A. Lapthorn, and M. Kadodwala, "Superchiral" spectroscopy: Detection of protein higher order hierarchical structure with chiral plasmonic nanostructures, J. Am. Chem. Soc. **137**, 8380 (2015).

[16] R. Y. Wang, P. Wang, Y. Liu, W. Zhao, D. Zhai, X. Hong, Y. Ji, X. Wu, F. Wang, D. Zhang, W. Zhang, R. Liu, and X. Zhang, Experimental observation of giant chiroptical amplification of small chiral molecules by gold nanosphere clusters, J. Phys. Chem. C **118**, 9690 (2014).

[17] T. Levi-Belenkova, A. O. Govorov, and G. Markovich, Orientation-sensitive peptide-induced plasmonic circular

dichroism in silver nanocubes, J. Phys. Chem. C **120**, 12751 (2016).

[18] W. Ma, H. Kuang, L. Xu, L. Ding, C. Xu, L. Wang, and N. A. Kotov, Attomolar, DNA detection with chiral nanorod assemblies, Nat. Commun. **4**, 2689 (2013).

[19] F. Lu, Y. Tian, M. Liu, D. Su, H. Zhang, A. O. Govorov, and O. Gang, Discrete nanocubes as plasmonic reporters of molecular chirality, Nano Lett. **13**, 3145 (2013).

[20] B. M. Maoz, R. van der Weegen, Z. Fan, A. O. Govorov, G. Ellestad, N. Berova, E. W. Meijer, and G. Markovich, Plasmonic chiroptical response of silver nanoparticles interacting with chiral supramolecular assemblies, J. Am. Chem. Soc. **134**, 17807 (2012).

[21] R. Verre, Z. J. Yang, T. Shegai, and M. Kall, Optical magnetism and plasmonic Fano resonances in metal-insulator-metal oligomers, Nano Lett. **15**, 1952 (2015).

[22] S. N. Sheikholeslami, A. Garcia-Etxarri, and J. A. Dionne, Controlling the interplay of electric and magnetic modes via Fano-like plasmon resonances, Nano Lett. **11**, 3927 (2011).

[23] M. Cortie and M. Ford, Plasmon-induced current loop in gold semi-shells, Nanotechnology **18**, 235704 (2007).

[24] S. Yoo and Q. Park, Chiral Light-Matter Interaction in Optical Resonators, Phys. Rev. Lett. **114**, 203003 (2015).

[25] M. H. Alizadeh and B. M. Reinhard, Plasmonically enhanced chiral optical fields and forces in achiral split ring resonators, ACS Photonics **2**, 361 (2015).

[26] A. Garcia-Etxarri and J. A. Dionne, Surface-enhanced circular dichroism spectroscopy mediated by nonchiral nanoantennas, Phys. Rev. B **87**, 235409 (2013).

[27] C. Kramer, M. Schäferling, T. Weiss, H. Giessen, and T. Brixner, Analytic optimization of near-field optical chirality enhancement, ACS photonics **4**, 396 (2017).

[28] W. Zhang, T. Wu, R. Wang, and X. Zhang, Surface-enhanced circular dichroism of oriented chiral molecules by plasmonic nanostructures, J. Phys. Chem. C **121**, 666 (2017).

[29] A. Pham, A. Zhao, C. Genet, and A. Drezet, Optical chirality density and flux measured in the local density of states of spiral plasmonic structures, Phys. Rev. A **98**, 013837 (2018).

[30] Y. Tang and A. E. Cohen, Optical Chirality and Its Interaction with Matter, Phys. Rev. Lett. **104**, 163901 (2010).

[31] Y. Tang and A. E. Cohen, Enhanced enantioselectivity in excitation of chiral molecules by superchiral light, Science **332**, 333 (2011).

[32] M. M. Coles and D. L. Andrews, Chirality and angular momentum in optical radiation, Phys. Rev. A **85**, 063810 (2012).

[33] J. S. Choi and M. Cho, Limitations of a superchiral field, Phys. Rev. A **86**, 063834 (2012).

[34] T. Davis and E. Hendry, Superchiral electromagnetic fields created by surface plasmons in nonchiral metallic nanostructures, Phys. Rev. B **87**, 085405 (2013).

[35] O. Neufeld, M. E. Tzur, and O. Cohen, Degree of chirality of electromagnetic fields and maximally chiral light, Phys. Rev. A **101**, 053831 (2020).

[36] A. Vazquez-Guardado and D. Chanda, Superchiral Light Generation on Degenerate Achiral Surfaces, Phys. Rev. Lett. **120**, 137601 (2018).

[37] M. Schäferling, X. Yin, N. Engheta, and H. Giessen, Helical plasmonic nanostructures as prototypical chiral near-field sources, ACS Photonics **1**, 530 (2014).

[38] Y. Liu, W. Zhao, Y. Ji, R. Wang, X. Wu, and X. Zhang, Strong superchiral field in hot spots and its interaction with chiral molecules, Europhys. Lett. **110**, 17008 (2015).

[39] M. Schäferling, *Chiral Nanophotonics* (Springer International, Berlin, 2017).

[40] M. Schäferling, N. Engheta, H. Giessen, and T. Weiss, Enantioselective chiral near-fields by diagonal slit and mirror configuration, ACS Photonics **3**, 1076 (2016).

[41] T. Wu, X. Zhang, R. Wang, and X. Zhang, Strongly enhanced Raman optical activity in molecules by magnetic response of nanoparticles, J. Phys. Chem. C **120**, 14795 (2016).

[42] C. S. Ho, A. Garcia-Etxarri, Y. Zhao, and J. Dionne, Enhancing enantioselective absorption using dielectric nanospheres, ACS Photonics **4**, 197 (2017).

[43] G. Pellegrini, M. Finazzi, M. Celebrano, L. Duò, and P. Biagioni, Chiral surface waves for enhanced circular dichroism, Phys. Rev. B **95**, 241402(R) (2017).

[44] W. Zhang, T. Wu, R. Wang, and X. Zhang, Amplification of the molecular chiroptical effect by low-loss dielectric nanoantennas, Nanoscale **9**, 5701 (2017).

[45] T. Wu, W. Zhang, R. Wang, and X. Zhang, A giant chiroptical effect caused by the electric quadrupole, Nanoscale **9**, 5110 (2017).

[46] M. L. Solomon, J. Hu, M. Lawrence, A. García-Etxarri, and J. A. Dionne, Enantiospecific optical enhancement of chiral sensing and separation with dielectric metasurfaces, ACS Photonics **6**, 43 (2018).

[47] E. Mohammadi, K. L. Tsakmakidis, A. N. Askarpour, P. Dehkhoda, A. Tavakoli, and H. Altug, Nanophotonic platforms for enhanced chiral sensing, ACS Photonics **5**, 2669 (2018).

[48] F. Graf, J. Feis, X. Garcia-Santiago, M. Wegener, C. Rockstuhl, and I. Fernandez-Corbaton, Achiral, helicity preserving, and resonant structures for enhanced sensing of chiral molecules, ACS Photonics **6**, 482 (2019).

[49] J. Hu, M. Lawrence, and J. A. Dionne, High quality factor dielectric metasurfaces for ultraviolet circular dichroism spectroscopy, ACS Photonics **7**, 36 (2019).

[50] X. Zambrana-Puyalto and N. Bonod, Tailoring the chirality of light emission with spherical Si-based antennas, Nanoscale **8**, 10441 (2016).

[51] I. Fernandez-Corbaton, X. Zambrana-Puyalto, N. Tischler, X. Vidal, M. L. Juan, and G. Molina-Terriza, Electromagnetic Duality Symmetry and Helicity Conservation for the Macroscopic Maxwell's Equations, Phys. Rev. Lett. **111**, 060401 (2013).

[52] I. Fernandez-Corbaton, Helicity and duality symmetry in light matter interactions: Theory and applications, in *Laser Science 2015* (Optical Society of America, Washington, DC, 2015), p. LM1H.2.

[53] M. Lawrence, N. Xu, X. Zhang, L. Cong, J. Han, W. Zhang, and S. Zhang, Manifestation of $\mathcal{PT}$ Symmetry Breaking in Polarization Space with Terahertz Metasurfaces, Phys. Rev. Lett. **113**, 093901 (2014).

[54] S. Yu, H. S. Park, X. Piao, B. Min, and N. Park, Low-dimensional optical chirality in complex potentials, Optica **3**, 1025 (2016).

[55] T. Wu, W. Zhang, H. Zhang, S. Hou, G. Chen, R. Liu, C. Lu, J. Li, R. Wang, P. Duan, J. Li, B. Wang, L. Shi, J. Zi, and X. Zhang, Vector Exceptional Points with Strong Superchiral Fields, Phys. Rev. Lett. **124**, 083901 (2020).

[56] S. Fan and J. D. Joannopoulos, Analysis of guided resonances in photonic crystal slabs, Phys. Rev. B **65**, 235112 (2002).

[57] S. G. Park, Y. Lee, S. Kwon, S. Yoo, Q. H. Park, J. K. Park, and K. H. Jeong, Extraordinary figure-of-merit of magnetic resonance from ultrathin silicon nanohole membrane as all-dielectric metamaterial, Adv. Opt. Mater. **5**, 1600628 (2017).

[58] J. Lee, B. Zhen, S. L. Chua, W. Qiu, J. D. Joannopoulos, M. Soljačić, and O. Shapira, Observation and Differentiation of Unique High-Q Optical Resonances Near Zero Wave Vector in Macroscopic Photonic Crystal Slabs, Phys. Rev. Lett. **109**, 067401 (2012).

[59] K. Sakoda, *Optical Properties of Photonic Crystals* (Springer Science & Business Media, Berlin, 2004).

[60] J. D. Joannopoulos, S. G. Johnson, J. N. Winn, and R. D. Meade, *Photonic Crystals: Molding the Flow of Light* (Princeton University Press, Princeton, NJ, 2008).

[61] W. Yan, P. Lalanne, and M. Qiu, Shape Deformation of Nanoresonator: A Quasinormal-Mode Perturbation Theory, Phys. Rev. Lett. **125**, 013901 (2020).

[62] See Supplemental Material at http://link.aps.org/supplemental/10.1103/PhysRevA.102.053519 for details of the explaining of the parabolic curve in Fig. 1(d), top view for distributions of electric and magnetic fields for the double-degenerate TM-like and TE-like modes.

[63] I. Fernandez-Corbaton, M. Fruhnert, and C. Rockstuhl, Objects of Maximum Electromagnetic Chirality, Phys. Rev. X **6**, 031013 (2016).